# Mathematical description of photobleaching in vivo describing the influence of tissue optics on measured fluorescence signals

Jongen, A.J.L.; Sterenborg, H.J.C.M.

DOI
10.1088/0031-9155/42/9/003

Publication date
1997

Published in
Physics in Medicine and Biology

Phys. Med. Biol. **42** (1997) 1701–1716. Printed in the UK PII: S0031-9155(97)79580-0

# Mathematical description of photobleaching *in vivo* describing the influence of tissue optics on measured fluorescence signals

Armand J L Jongen† and Henricus J C M Sterenborg

Laser Centre, Academic Medical Centre, PO Box 2270, 1100 DE Amsterdam, The Netherlands

Received 14 November 1996, in final form 29 May 1997

**Abstract.** The observed decrease in the fluorescence signal during photodynamic therapy (PDT) may contain dosimetric information as this photobleaching provides direct information on the photodynamic processes occurring in the tissue. A correct interpretation of the photobleaching signal, however, is crucial for its use in dosimetry. In this study the influence of scattering and absorption phenomena in tissue on the emitted fluorescence signal are described mathematically. Analytical solutions of the resulting expression show a difference from the single-decaying-exponential function generally used for describing photobleaching signals. The solutions are a function of the fluence rate at the inner side of the tissue boundary $\Psi_0^*$, the photobleaching dose constant $\beta$, the incident irradiation power $I_0$ and time. The accuracy of the results was investigated by comparison of the analytic solutions with numerical calculations using fluence rate profiles and escape functions obtained by Monte Carlo (MC) simulations. Good resemblance is observed when the value for $\Psi_0^*$ calculated by the MC simulations is used in the analytical solutions. Experimental results in this study indicate the photobleaching dose constant of ALA-induced PpIX to be $33 \pm 3$ J cm$^{-2}$. Determination of $\beta$ for different types of photosensitizer and the development of an accurate method to determine $\Psi_0^*$ can make monitoring of photobleaching during PDT valuable for dosimetry.

## 1. Introduction

Photodynamic therapy (PDT) is a new treatment modality for superficial tumours. It is a two-step treatment consisting of the administration of a tumour-localizing photosensitizer followed some time later by light exposure. Photochemical activation of the sensitizer then leads to the destruction of the malignant tissue.

Photosensitizers also show fluorescence after excitation. Fluorescence intensities normally decrease during PDT. The decrease of the fluorescence signal observed during PDT has been related to the therapeutic inactivation or alternation of the photosensitizer (Moan 1986). This temporal decrease of the fluorescence signal is normally referred to as photobleaching. Photobleaching during PDT is shown to result in a loss of reciprocity between drug and light dose. It also induces an upper limit on the photodynamic effect (Potter *et al* 1987). This limiting effect of photobleaching on photosensitizer activity can be used to reduce skin photosensitivity (Boyle and Potter 1987, Roberts *et al* 1989).

Although photobleaching may be considered a complication in PDT, the related decrease of the fluorescence signal also provides information on the photodynamic processes

† To whom correspondence should be addressed

0031-9155/97/091701+16$19.50  

occurring in the tissue. Therefore, the temporal behaviour of the fluorescence during PDT may provide valuable dosimetric information (Grossweiner 1991, Svaasand and Potter 1992). However, correct interpretation of this behaviour is necessary for accurate application of this information.

Photobleaching has been shown to be a first-order mechanism with respect to the locally experienced light exposure (Mang *et al* 1987). When the photosensitizer concentration is assumed to be proportional to the fluorescence signal (Potter and Mang 1984), the temporal behaviour of the fluorescence is expected to follow first-order kinetics. In practice, however, fluorescence measurements *in vivo* appear to follow a higher-order curve. These higher-order effects could be caused by several different fluorophore types that bleach with different time constants (Zeng *et al* 1993), resulting from the formation of additional fluorescing photoproducts (König *et al* 1990, Dietel *et al* 1990), or due to damage of cell membrane lipids, reducing necessary binding sites to activate photosensitizer molecules (Moan 1988).

In this paper we will show that in a photosensitized turbid medium, tissue optics influences the emitted fluorescence light in such a way that it can no longer be described by a single exponential, even if there are *no* higher-order effects and only one fluorescing photosensitizer is present. However, use of additional exponentials with different time constants to describe the measured signal is not necessary.

A mathematical description for the emitted fluorescence signal of a photosensitized turbid medium is derived. This description is based on first-order photoinactivation and uses one bleaching time constant that corresponds to one fluorescing photoactive component. The resulting integral has no general closed form solution but in some discrete cases, analytical solutions can be found. All practical useful solutions show a divergence from a single exponential.

In order to evaluate the accuracy of the analytical solutions found, they will be compared with numerical solutions of the original integral. The analytical solutions will then be used to fit experimental data that are obtained by photobleaching measurements *in vivo*. Since these solutions still contain physical information, fitting will provide information about variables relevant for the mechanism of photobleaching. Performed fits in this study result in an indication for the bleaching time constant of the used photosensitizer (PpIX in our case: see section 3.2). These results, together with the information the mathematical description provides about the mechanisms involved in photobleaching, may enable the use of photobleaching monitoring as a dosimetric tool in clinical PDT.

## 2. Mathematical description

Consider a turbid medium containing a bleachable fluorescent photosensitizer. Let the concentration of identical fluorescing photosensitizer molecules at place $\boldsymbol{r}$ be described by $C(\boldsymbol{r}, t)$. This concentration is assumed small enough to avoid effects on the absorption coefficient of the tissue. Irradiation of this medium with a constant homogeneous incident power $I_0$ [W m$^{-2}$] results in a time independent fluence rate distribution $\Psi(\boldsymbol{r})$ [W m$^{-2}$] that is linear with respect to $I_0$. Due to photobleaching the local concentration of fluorescing molecules decreases. Assuming photobleaching to be a first-order process, the rate at which the concentration $C(\boldsymbol{r}, t)$ decreases is proportional to the locally experienced fluence rate $\Psi(\boldsymbol{r})$. Thus

$$\frac{\partial C(\boldsymbol{r}, t)}{\partial t} \propto -\beta^{-1}\Psi(\boldsymbol{r})C(\boldsymbol{r}, t) \tag{1}$$

where $\beta$ [J m$^{-2}$] is the photobleaching dose constant.

The locally generated photosensitizer fluorescence $f(\boldsymbol{r}, t)$ is proportional to the excited state production. Neglecting two-step excitations and other higher-order effects, this production is proportional to $\Psi(\boldsymbol{r})$ and to the local concentration photosensitizer $C(\boldsymbol{r}, t)$. Therefore

$$f(\boldsymbol{r}, t) \propto \Psi(\boldsymbol{r}) C(\boldsymbol{r}, t). \tag{2}$$

Solving the differential equation (1) and inserting the result into (2) yields

$$f(\boldsymbol{r}, t) \propto \Psi(\boldsymbol{r}) C(\boldsymbol{r}, 0) \exp\left(-\beta^{-1} \Psi(\boldsymbol{r}) t\right) \tag{3}$$

where $C(\boldsymbol{r}, 0)$ is the initial local photosensitizer concentration at time $t = 0$ when irradiation started.

The total fluorescence light emitted by a volume $V$ from place $(x, y)$ on the surface $S$ is given by

$$F(x, y, t) = \int\int_V\int f(\boldsymbol{r}, t) \zeta^*(x, y, \boldsymbol{r}) \, \mathrm{d}\boldsymbol{r}. \tag{4}$$

Here the dimensionless factor $\zeta^*(x, y, \boldsymbol{r})$ is the so-called escape function describing the probability that a photon generated at $\boldsymbol{r}$ leaves the surface at $(x, y)$.

We assume an initially homogeneously distributed photosensitizer concentration. Then $C(\boldsymbol{r}, 0)$ is constant, independent of $\boldsymbol{r}$ and can be substituted by $C_0$. Furthermore, using a broad-beam approximation, (4) can be substituted by its one-dimensional equivalent

$$F(t) = \eta C_0 \int_0^\infty \Psi(z) \exp\left(-\beta^{-1} \Psi(z) t\right) \zeta^*(z) \, \mathrm{d}z \tag{5}$$

where the expression for $f(z, t)$ given by (3) is inserted and $\eta$ is a constant proportionality factor describing the fluorescence quantum yield.

We now introduce a dimensionless fluence rate $\Psi^*(z) = \Psi(z)/I_0$, where $I_0$ is the incident power, and substitute $\beta(I_0)^{-1}$ by the bleaching time constant $\tau$ [s]. Then we can calculate $F(t)$ without knowing or assuming anything about $\tau$ other than that it is constant for a certain type of photosensitizer and constant $I_0$.

Furthermore, when defining the relative fluorescence function $\mathcal{F}(t)$ as

$$\mathcal{F}(t) = F(t)/F(0) = \int_0^\infty \Psi^*(z) \exp\left[-\Psi^*(z) \, (t/\tau)\right] \zeta^*(z) \, \mathrm{d}z \left(\int_0^\infty \Psi^*(z) \zeta^*(z) \, \mathrm{d}z\right)^{-1} \tag{6}$$

we have an expression that is independent of $\eta$, of $C_0$ and of $I_0$.

There is no closed form solution of (6). Fluence rate distributions, as well as escape functions, usually have forms that prohibit straightforward analytical solutions.

To determine the bleaching time constant $\tau$ however, which describes the basic photobleaching process at molecular level, we would like to fit an analytic solution to fluorescence measurement data.

In order to accomplish this we will substitute analytic approximations for the fluence rate profile and escape function that enable analytic solutions of (6). The accuracy of these solutions will be evaluated by comparing them with numerical calculations of (6) that use fluence rate profiles and escape functions obtained by Monte Carlo (MC) simulations.

### *2.1. Analytical solutions*

Analysing (6) showed that there are only analytical solutions possible if $\Psi^*(z)$ and $\zeta^*(z)$ are single-exponential functions. Hence we approximate the fluence rate and the escape

function by

$$\begin{aligned}\Psi^*_{\mathrm{AA}}(z) &= \Psi^*_0 \exp\left(-\mu_{\mathrm{eff}}(\lambda_{\mathrm{exc}})z\right)\\ \zeta^*_{\mathrm{AA}}(z) &= \zeta^*_0 \exp\left(-\mu_{\mathrm{eff}}(\lambda_{\mathrm{det}})z\right)\end{aligned} \tag{7}$$

where $\mu_{\mathrm{eff}}(\lambda_{\mathrm{exc}})$ and $\mu_{\mathrm{eff}}(\lambda_{\mathrm{det}})$ are the effective attenuation coefficients for the excitation and detection wavelength respectively and the subscript AA denotes that the functions are analytical approximations.

One must bear in mind that especially in the superficial part of an irradiated turbid medium this may not be a very good approximation since the fluence rate profile can contain a maximum there. Furthermore the factor $\Psi^*_0$ does not generally equal unity since in a turbid medium the fluence rate at the inside of the boundary is higher than the irradiance of the incoming beam (Star 1997).

Inserting (7) in (6) yields

$$\mathcal{F}(t) = \int_0^\infty \exp\left[-(\mu_{\mathrm{e}}+\mu_{\mathrm{d}})\,z\right]\exp\left[-\Psi^*_0\,(t/\tau)\,\mathrm{e}^{-\mu_{\mathrm{e}}z}\right]\mathrm{d}z\left\{\int_0^\infty \exp\left[-(\mu_{\mathrm{e}}+\mu_{\mathrm{d}})\,z\right]\mathrm{d}z\right\}^{-1} \tag{8}$$

where we have abbreviated $\mu_{\mathrm{eff}}(\lambda_{\mathrm{exc}})$ and $\mu_{\mathrm{eff}}(\lambda_{\mathrm{det}})$ to $\mu_{\mathrm{e}}$ and $\mu_{\mathrm{d}}$ respectively. Analytical solutions for this equation can be found for the cases where $\mu_{\mathrm{d}} = n\mu_{\mathrm{e}}$, with $n$ or $(n+\frac{1}{2})$ an integer (see appendix). They are given by

$$\mathcal{F}_n(t) = \begin{cases} (n+1)!\left[\dfrac{1}{\Psi^*_0\,(t/\tau)}\right]^{n+1}\left\{1-\exp\left[-\Psi^*_0\,(t/\tau)\right]\right\} \\ \qquad -\dfrac{\exp\left[-\Psi^*_0\,(t/\tau)\right]}{\Psi^*_0\,(t/\tau)}\displaystyle\sum_{k=0}^{n-1}\frac{(n+1)!}{(n-k)!}\left[\frac{1}{\Psi^*_0\,(t/\tau)}\right]^k & n\in\mathbb{N} \\ \dfrac{(2n+2)!!}{2^{n+\frac{1}{2}}}\left[\dfrac{1}{\Psi^*_0\,(t/\tau)}\right]^{n+1}\dfrac{\sqrt{\pi}}{2}\,\mathrm{erf}\left[\sqrt{\Psi^*_0\,(t/\tau)}\right] \\ \qquad -\dfrac{\exp\left[-\Psi^*_0\,(t/\tau)\right]}{\Psi^*_0\,(t/\tau)}\displaystyle\sum_{k=0}^{n-\frac{1}{2}}\frac{(2n+2)!!}{(2n-2k)!!}\frac{1}{2^{k+1}}\left[\frac{1}{\Psi^*_0\,(t/\tau)}\right]^k & n+\tfrac{1}{2}\in\mathbb{N} \end{cases} \tag{9}$$

where erf[] denotes the tabulated error function and $m!! = m(m-2)\ldots\times 3\times 1$.

The function $\mathcal{F}_n(t)$ is independent of the actual optical parameters $\mu_{\mathrm{e}}$ and $\mu_{\mathrm{d}}$. It only depends on the ratio of these coefficients. These results imply that measurements of relative fluorescence signals in media with different $\mu_{\mathrm{e}}$ and $\mu_{\mathrm{d}}$ but equal ratios, or similarly using different excitation and detection wavelengths that result in an equal $n$, will show the same time dependence.

It can be shown from (9) that the relative fluorescence $\mathcal{F}_n(t)$ is described by a single exponential only when $n\to\infty$, i.e. the effective attenuation coefficient for the excitation light $\mu_{\mathrm{e}}$ equals zero. The fluence rate $\Psi^*(z)$ is then constant throughout the whole tissue, a case not encountered in normal practice.

To obtain the analytical solutions for $\mathcal{F}(t)$ in (6) we have approximated $\Psi^*(z)$ and $\zeta^*(z)$ by (7) and assumed the ratio of $\mu_{\mathrm{e}}$ and $\mu_{\mathrm{d}}$ to equal $n$ or $(n+\frac{1}{2})$, with $n$ an integer number. In order to evaluate the influence these approximations have on the results of (6), the solutions presented by (9) are compared with numerical calculations of (6) where the fluence rate profile and escape function obtained by MC simulations are used.

### *2.2. Evaluation of analytical solutions*

Using the absorption and reduced scattering coefficients for healthy rat skin tissue given in table 1 (Jacques *et al* 1993), MC simulations result in a fluence rate profile $\Psi^*_{\mathrm{MC}}(z)$ and escape function $\zeta^*_{\mathrm{MC}}(z)$ as depicted in figure 1.

**Table 1.** Optical parameters for healthy rat tissue used for MC simulations. The absorption coefficient $\mu_a$ and reduced scattering coefficient $\mu_s(1-g)$ are given for the excitation (630 nm) and detection (705 nm) wavelength respectively. Corresponding effective attenuation coefficients $\mu_{\mathrm{eff}}$ are calculated using $\mu_{\mathrm{eff}} = \{3\mu_a[\mu_a + \mu_s(1-g)]\}^{1/2}$. Adapted from Jacques *et al* (1993).

| Wavelength [nm] | $\mu_a$ [cm$^{-1}$] | $\mu_s(1-g)$ [cm$^{-1}$] | $\mu_{\mathrm{eff}}$ [cm$^{-1}$] |
|---|---|---|---|
| Excitation 630 | 0.23 | 21 | 3.83 |
| Detection 705 | 0.23 | 17 | 3.45 |

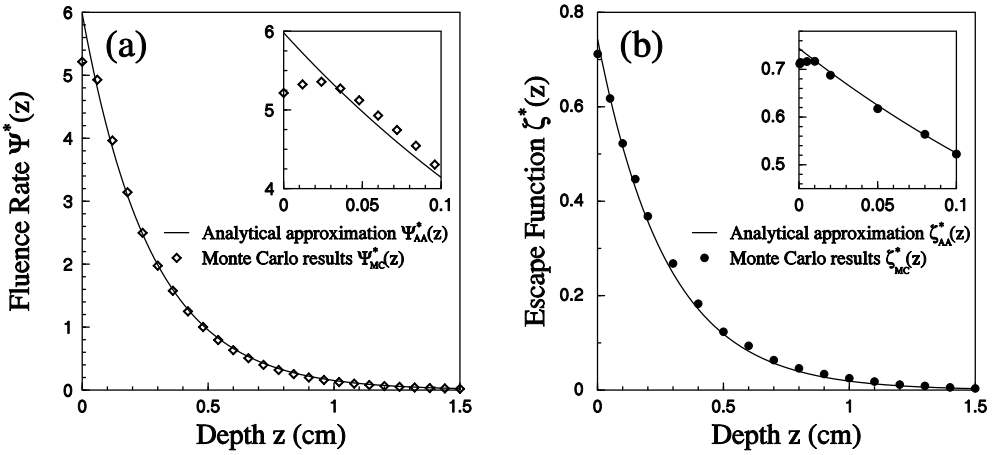


**Figure 1.** (a) Fluence rate profile $\Psi^*_{\mathrm{MC}}(z)$, and (b) escape function $\zeta^*_{\mathrm{MC}}(z)$ obtained by MC simulations (◇ and ● respectively) where the tissue optics parameters of table 1 are used. These MC results are approximated by the $\Psi^*_{\mathrm{AA}}(z)$ and $\zeta^*_{\mathrm{AA}}(z)$ as given in (7) (——). Values for $\Psi^*_0$ and $\mu_e$ are determined using a least-squares fit resulting in $\Psi^*_0 = 5.98 \pm 0.01$ and $\mu_e = 3.67 \pm 0.01$ cm$^{-1}$. Setting the ratio of $\mu_e$ and $\mu_d$ equal to one results in the drawn escape function $\zeta^*_{\mathrm{AA}}(z)$. For $\Psi^*_{\mathrm{MC}}(z)$ more points were available for the calculations but they are discarded from the graphs for reasons of clarity. The corresponding intermediate points for $\zeta^*_{\mathrm{MC}}(z)$ were determined by non-linear interpolation.

Calculating the least-squares sum of the difference between the MC fluence rate profile $\Psi^*_{\mathrm{MC}}(z)$ and $\Psi^*_{\mathrm{AA}}(z)$ from (7) results in values for $\Psi^*_0$ and $\mu_e$. The calculated value for $\Psi^*_0$ equals $5.98 \pm 0.01$ and $\mu_e = 3.67 \pm 0.01$ cm$^{-1}$ for this set of optical parameters.

We now have to choose an appropriate $n$ in order to choose one of the solutions presented in (9) that best describes the considered problem. From table 1 it is seen that the ratio of $\mu_e$ and $\mu_d$ is nearly unity, allowing us to set $n$ in (9) to one. Setting $n$ to equal one implies that $\mu_d$ in (7) equals $\mu_e$, i.e. $\mu_d = 3.67$. This results in an escape function $\zeta^*_{\mathrm{AA}}(z)$ as pictured in figure 1(b). Because $\mu_d$ used to construct $\zeta^*_{\mathrm{AA}}(z)$ is larger than the $\mu_d$ used for the MC simulations (see table 1), $\zeta^*_{\mathrm{AA}}(z)$ is smaller than $\zeta^*_{\mathrm{MC}}(z)$ for most depths $z$.

We now can calculate $\mathcal{F}_1(t)$ from (9) and numerically determine $\mathcal{F}(t)$ given by (6) with

$\Psi^*(z)$ and $\zeta^*(z)$ used from the MC results. The results of these calculations are presented in figure 2 where the relative fluorescence decrease $\mathcal{F}(t)$ is plotted as a function of $t/\tau$.

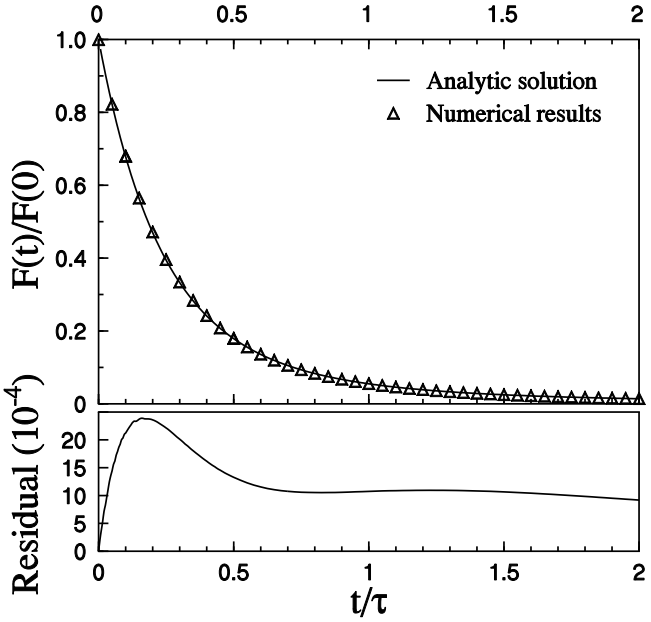


**Figure 2.** $\mathcal{F}(t)$ as a function of $t/\tau$ determined by (9) (——) and numerical calculations of (6) using MC results for $\Psi^*(z)$ and $\zeta^*(z)$ (△). More numerical points were calculated and used to construct the residual graph. Due to the equalization of $\mu_e$ and $\mu_d$, the escape function $\zeta^*_{AA}(z)$ underestimated $\zeta^*_{MC}(z)$. This results in a relative fluorescence signal $\mathcal{F}_1(t)$ that is always smaller than the numerically calculated $\mathcal{F}(t)$. Hence the residuals of the analytical results from the numerical calculations are all positive with with a maximum of 0.24% at $t/\tau = 0.16$.

There is very little difference between the results of the analytical solutions and the numerical calculations using the results of MC simulations. The residuals that are plotted in the lower part of the graph show that the difference is less than 0.24% for $0 \leqslant t/\tau \leqslant 2$. All residuals are positive because the analytical approximation for the escape function $\zeta^*_{AA}(z)$ underestimates $\zeta^*_{MC}(z)$ due to the equalization of $\mu_e$ and $\mu_d$. The graph, however, does not represent a fit but illustrates the influence the approximations made while deriving (9) have on the final result. As this influence appears to be small for the case examined we are confident that measured photobleaching signals can be described accurately by (9) and fitting of experimental data can provide a reliable indication for $\tau$ and thus for $\beta$.

Determination of $\Psi^*_0$ for every different situation however, remains a problem. The values available for tissue optics parameters of human skin *in vivo* vary (Cheong *et al* 1990), so MC simulations that use these parameters cannot provide accurate values for $\Psi^*_0$ in every situation. Furthermore, there were no other methods available to us that could determine or measure $\Psi^*_0$. Since the wavelengths we are going to use in our experiments are close to those listed in table 1 we will use the value for $\Psi^*_0$ determined above with the aid of MC simulations, i.e. $\Psi^*_0 = 5.98$, and set $n$ in (9) equal to one. The implications all this has on the results obtained in this work will be discussed in section 5.

## 3. Experiments

The tools developed in section 2 enable us to determine a single bleaching time constant of a particular photosensitizer *in vivo* by fitting experimental results as described below.

### *3.1. Experimental setup*

The output wavelength of a tunable argon-dye laser was tuned to 630 nm. The excitation light was delivered to the target tissue through a fibre optical system which enabled variation of the spot size. The distance from the fibre optical system to the target tissue was kept constant. The output power of the dye laser was set and stabilized by a feedback loop to let the incident power density of the excitation light on the tissue equal 150 mW $cm^{-2}$.

Fluorescence light from the tissue traverses a high-pass glass filter (Schott RG665) which absorbs light at wavelengths shorter than 665 nm. The remaining fluorescence light is then collected by a monochrome CCD camera (Sony) that passes a video-signal of the fluorescence image to an attached workstation (Silicon Graphics Inc.). Here the image is digitized and stored at a frame rate of one image per second. After that, specially developed software is used for image analysis.

Determination of the fluorescence intensity as a function of time is done by choosing a region of interest (ROI) in the digitized image. Setting a threshold pixel value for this ROI enables selection of arbitrarily shaped surface. The calculated mean pixel value and standard error of the mean (SE) of this surface are stored for each image resulting in a file containing the related fluorescence intensity as a function of time. Care is taken to keep the shape and area of the selected surface constant in time.

Fluorescence measurements were performed during PDT on patients with condyloma acuminatum, on the dorsal skin and tail of healthy rats, and on patients with Kaposi's sarcoma.

### *3.2. Photosensitizer*

For both measurements on patients and rats, 5-aminolevulinic acid (ALA) was used to photosensitize the tissue. ALA is not a photosensitizing agent itself, but an immediate precursor of several porphyrins in the biosynthesis of haem (Kennedy and Pottier 1992). By administration of ALA in excess, the intracellular concentration of protoporphyrin IX (PpIX), a potent photosensitizer, is temporarily increased.

The ALA was administered to the patients topically on the target tissue in a 20% solution of Instillagel 8–16 hours prior to illumination.

The rats were injected i.p. with 100 mg/kg body weight of ALA, 4 hours prior to illumination and completely anaesthetized by i.m. injection of a mixture containing ketamine (90 mg/kg body weight), xylazine (10 mg/kg body weight) and atropine (0.05 mg/kg body weight).

### *3.3. Data analysis*

Fluorescent molecules are naturally present in almost every type of tissue. Therefore fluorescence signals measured *in vivo* also contain a contribution that arises from this so-called autofluorescence. If we assume that the autofluorescence does not bleach we can modify (9) to account for this. A practically useful expression for fitting data then yields

$$F(t)/F(0) = (\mathcal{F}_n(t) + A/F(0)) \,/\, (1 + A/F(0)) \tag{10}$$

where $A$ denotes the autofluorescence, considered constant in time, and $F(t)$ is the absolute measured fluorescence signal as function of time.

The data obtained from experiments have to be fitted with the solution $\mathcal{F}_1(t)$ as the used wavelengths for excitation and detection have an effective attenuation ratio of nearly one. When the above correction is made the final expression used for fitting reads

$$F(t) = \Big(2\left[\Psi_0^*(t/\tau)\right]^{-2}\left\{1-\exp\left[-\Psi_0^*(t/\tau)\right]\right\} - 2\left[\Psi_0^*(t/\tau)\right]^{-1}\exp\left[-\Psi_0^*(t/\tau)\right]+\mathcal{A}\Big)(1+\mathcal{A})^{-1}F(0) \tag{11}$$

where $\Psi_0^*/\tau$, $\mathcal{A}$ $(= A/F(0))$ and $F(0)$ are used as fit parameters and $F(t)$ equals the determined average pixel value.

Although $A$ is considered constant in time for one single measurement, it should be noted that there can be differences in the initial absolute measured fluorescence arising from the photosensitizer $F(0)$ between different measurements due to variations in initial concentrations of the photosensitizer, even if these measurements are performed on the same type of tissue. Therefore we will not expect the fit parameter $\mathcal{A}$ to be constant for all measurements.

To determine the starting parameter values for the fit we calculated the initial decrease of the relative experimental fluorescence signal. If we differentiate (6) with respect to $t$, use the relation $\mu_\mathrm{d} = n\mu_\mathrm{e}$ and take the limit for $t \to 0$ the initial relative decrease of $\mathcal{F}_n(t)$ yields

$$\lim_{t\to 0}\frac{\partial \mathcal{F}_n(t)}{\partial t} = -\frac{\Psi_0^*}{\tau}\frac{(n+1)}{(n+2)}. \tag{12}$$

Taking this same limit for the experimental data yields

$$\lim_{t\to 0}\frac{\partial\left(F(t)/F(0)\right)}{\partial t} = \lim_{t\to 0}\frac{\partial \mathcal{F}_n(t)}{\partial t}(1+\mathcal{A})^{-1} = \left(-\frac{\Psi_0^*}{\tau}\frac{(n+1)}{(n+2)}\right)(1+\mathcal{A})^{-1}. \tag{13}$$

Estimation of $\mathcal{A}$, setting $n$ to one and equalizing the experimental value $F(t)/F(0)$ and (13) results in a value for $\Psi_0^*/\tau$ that can be used as a starting value for the actual fit.

## 4. Results

### *4.1. Condyloma acuminatum*

The fluorescence measurements performed during PDT of patients with condyloma acuminatum (CA) were sometimes troubled by movement artefacts. In some cases abrupt movements from or towards the camera occur. This results in a sudden decrease or increase of the measured fluorescence intensities. If the original position is resumed the deviating data points can be left out of the fit. When the new position is maintained for a longer time data correction is possible. An example of such a correction is given in figure 3.

Average pixel values for a strongly fluorescing region were determined for each image in an image sequence from zero to 200 seconds. A least-squares sum fit was then performed using (11) as the fit function, with initial values for the fit parameters as calculated with (13).

Values for $\Psi_0^*/\tau$ and $\mathcal{A}$ obtained this way after fitting experimental data obtained during measurements of four patients with CA are given in table 2. The third fit parameter $F(0)$ is omitted in this table as no absolute fluorescence was measured and therefore

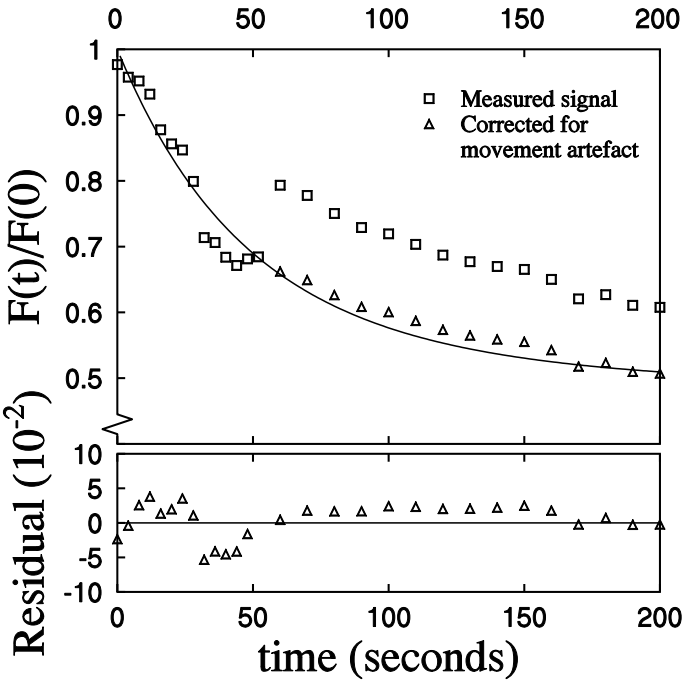


**Figure 3.** Results of a fluorescence measurement during PDT on a patient with CA where the relative average pixel values are shown (□). A sudden increase of the fluorescence intensity, concurrently with the observation of a sudden movement by the patient produces a movement artefact in the measured signal. Since the movement is abrupt and the new position is maintained, the data following the movement could be matched to the previous ones (△). A least-squares sum fit on these data with the expression given by (10) yields the drawn function (——) where $\Psi_0^*/\tau$ and $\mathcal{A}$ are $(29 \pm 1) \times 10^{-3}\mathrm{s}^{-1}$ and $0.92 \pm 0.02$ respectively. The third fit-parameter $F(0)$ is used to normalize the data. Residuals are given in the lower part of the figure. For reasons of clarity not all data points (one per second) are shown.

comparison of this parameter for different measurements is meaningless. It is however used for normalization of the data.

### *4.2. Healthy rat skin*

Fluorescence measurements were also performed on the skin of healthy anaesthetized rats to avoid movement artefacts. Two rats were used and both were irradiated twice. Again the average pixel value of a chosen spot was calculated for an image sequence from 0 to 200 seconds. The corresponding relative fluorescence intensity for a measurement on the dorsal skin is plotted in figure 4.

Calculated results from three other fluorescence measurements on rat skin are given in table 2. Numbers 1 and 2 are results of measurements on the first rat, numbers 3 and 4 on the second. The results of number 4 were obtained from a fluorescence measurement on the rat's tail. The measurements are seen to be much more stable than the ones on patients. Consequently the residuals between the fit and the experimental data are an order of magnitude smaller than in figure 3 and figure 5 ($10^{-3}$ instead of $10^{-2}$).

**Table 2.** Values for $\Psi_0^*/\tau$ and $\mathcal{A}$ resulting from least-squares sum fits performed on measured data. The numbers following the ± symbols are the standard deviations in the fit parameters as calculated by the fitting procedure. The results are grouped by the kind of target tissue and different measurements in each group are numbered. Average values for $\Psi_0^*/\tau$ for the different groups are given with the standard error of the mean. The variations in $\mathcal{A}$ will be discussed in section 5.

| | Condyloma ac. | | Healthy rat skin | | Kaposi's sarcoma | |
|---|---|---|---|---|---|---|
| No | $\Psi_0^*/\tau$ [$10^{-3}$ $s^{-1}$] | $\mathcal{A}$ — | $\Psi_0^*/\tau$ [$10^{-3}$ $s^{-1}$] | $\mathcal{A}$ — | $\Psi_0^*/\tau$ [$10^{-3}$ $s^{-1}$] | $\mathcal{A}$ — |
| 1 | $22.6 \pm 0.7$[a] | $3.48 \pm 0.04$ | $27.6 \pm 0.3$ | $0.729 \pm 0.005$ | $7.3 \pm 0.5$ | $2.1 \pm 0.1$ |
| 2 | $29 \pm 1$ | $0.92 \pm 0.02$ | $29 \pm 1$ | $5.03 \pm 0.09$ | $4.1 \pm 0.3$ | $0.76 \pm 0.07$ |
| 3 | $20.2 \pm 0.6$ | $2.38 \pm 0.04$ | $25.4 \pm 0.1$ | $0.700 \pm 0.002$ | $4.5 \pm 0.7$ | $0.9 \pm 0.1$ |
| 4 | $12.0 \pm 0.8$ | $0.47 \pm 0.04$ | $35 \pm 2$[b] | $4.8 \pm 0.1$ | $9 \pm 2$[a] | $1.9 \pm 0.2$ |
| Average | $21.0 \pm 3.5$ | | $29.3 \pm 2.0$ | | $6.2 \pm 1.2$ | |

[a] Measured data are corrected for movement artefacts.
[b] Fluorescence measured on the tail.

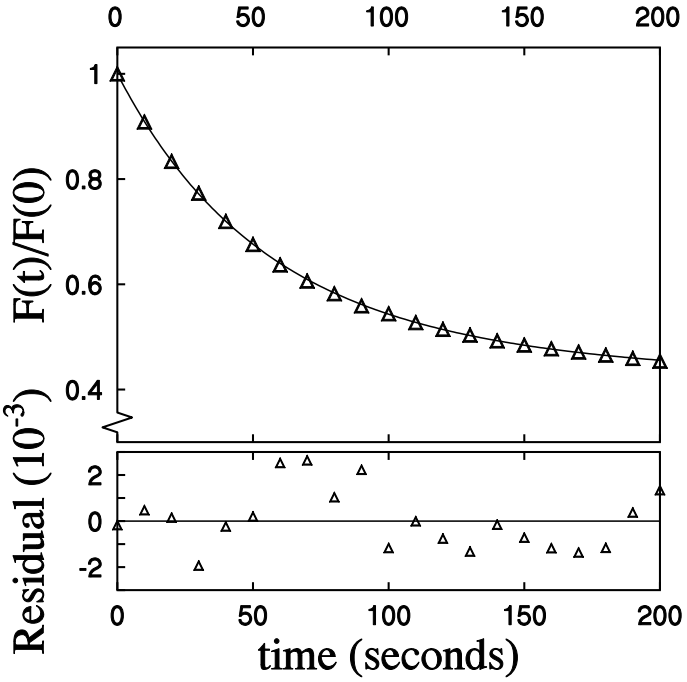


**Figure 4.** Relative fluorescence intensity as a function of time measured during irradiation of the dorsal skin of a healthy rat. Calculated fit parameters are $\Psi_0^*/\tau = (25.4 \pm 0.1) \times 10^{-3} s^{-1}$ and $\mathcal{A} = 0.700 \pm 0.002$.

### *4.3. Kaposi's sarcoma*

Additional measurements were performed on patients with Kaposi's sarcoma (KS) that were treated with PDT. As the lesions are situated on the arms and trunk of the patients, gradual movements can be avoided more easily than during PDT on patients with CA. An example

of a fluorescence measurement on a patient with KS and the result of the performed fit are shown in figure 5. The results of all performed fits are tabulated in table 2.

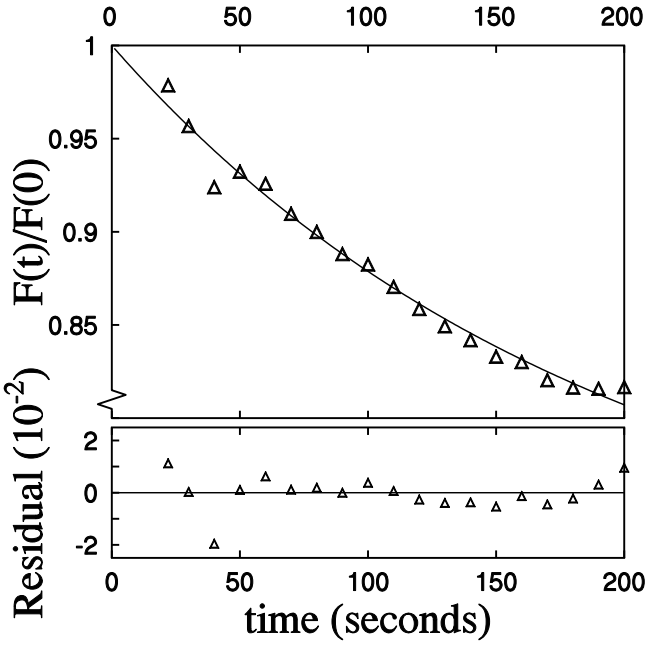


**Figure 5.** Fluorescence measurement during PDT of a Kaposi sarcoma. $\Psi_0^*/\tau = (7.3 \pm 0.5) \times 10^{-3}\mathrm{s}^{-1}$ and $\mathcal{A} = 2.1 \pm 0.1$.

## 5. Discussion

It is shown mathematically in this paper that the temporal behaviour of the relative fluorescence signal during PDT is not described by a single decaying exponent but follows a more complicated behaviour as described by (9). To get a feeling for the physical background of this solution one can think of several layers in a turbid medium that contribute to the resulting fluorescence signal separately. A deeper-lying layer will contribute less to the total fluorescence signal than a more superficial layer, as the exciting fluence rate is less at that position and the escape function is smaller. Since there is less light the rate at which the photosensitizer is bleached will also be lower. Consequently, the relative fluorescence signal from deeper-lying layers will appear at the surface as smaller signals that decay slower while the signals from the superficial layers are stronger and decay faster. The measured signal however, is the sum of all layers and its temporal behaviour is described by (9).

The values for $\Psi_0^*/\tau$ and $\mathcal{A}$ as calculated from the least-squares fits on measured data, summarized in table 2, show a large variability in the values for $\mathcal{A}$, the ratio of the initial absolute fluorescence signal and the remaining autofluorescence, even within one group. For the CA and KS measurements this might be related to a difference in ALA uptake between the different patients due to variations in skin composition and different application times (8–16 hours). This induces variations in the initial absolute fluorescence signal arising from the photosensitizer $F(0)$ and thus in $\mathcal{A}$.

Measurements performed on the dorsal skin (1, 2 and 3) and the tail (4) of two healthy rats also show a large variability in $\mathcal{A}$. There was 1 hour and 15 minutes between the first measurement on each rat (1 and 3) and the second (2 and 4). During this time the rats were exposed to background light from the room illumination and scattered light from the laser. Bleaching of the photosensitizer as a consequence of this light exposure could explain the higher values for $\mathcal{A}$ in measurements 2 and 4. This premature bleaching will induce a lower $F(0)$ and consequently a higher value for $\mathcal{A}$.

The calculated values for $\Psi_0^*/\tau$ are fairly consistent for each separate group apart from number 4 in the CA results. The sum of squares for this fit, however, was a factor of 30 higher than for the other measurements. Gradual movement artefacts that could not be detected from the fluorescence images or the measurement data (see section 4) might give an explanation for this difference.

Between the different groups the differences in calculated values for $\Psi_0^*/\tau$ are apparent. For the measurements made on patients with KS these values differ consequently from those obtained from patients with CA and from the healthy rats. As the used irradiation powers are equal for all measurements this is not what we would have expected. A possible explanation for this difference lies in the fact that a KS is a strongly vascularized tissue. The absorption for the excitation light (630 nm) in blood is much higher than in normal tissue (14.3 $\mathrm{cm}^{-1}$ versus 0.23 $\mathrm{cm}^{-1}$ (Cheong *et al* 1990)). Consequently the $\Psi_0^*$ is lower as will be the fitted parameter $\Psi_0^*/\tau$.

The optical parameters for CA tissue and healthy rat tissue also differ and thus so will $\Psi_0^*$ and $n$ for these cases. If we want to give an indication for the photobleaching dose constant $\beta$ of PpIX we had better only use the values calculated from fitting the measured fluorescence signal during irradiation of the healthy rat dorsal skin as the calculated value for $\Psi_0^*$ will be reliable for this case. Therefore we will also omit result number 4 in calculating an indication for $\beta$ as this measurement was made on the tail of the rat.

Doing so results in an average value for $\Psi_0^*/\tau$ of $(27 \pm 1) \times 10^{-3}$ $\mathrm{s}^{-1}$. With $\Psi_0^* = 5.98$ this yields $\tau = 219$ s at an irradiance $I_0$ of $150 \pm 10$ mW $\mathrm{cm}^{-2}$. As $\tau = \beta(I_0)^{-1}$ this results in a value for the photobleaching dose constant $\beta$ of $(33 \pm 3)$ J $\mathrm{cm}^{-2}$.

From this calculation it is clearly seen that the determination of $\beta$ is strongly dependent on the relative fluence rate on the inner side of the tissue boundary $\Psi_0^*$. In fact the accuracy of the value for $\tau$, and thus for $\beta$, determined from the fitting is as good as is the value for $\Psi_0^*$ calculated with the use of MC simulations as done in section 2.1.

An accurate determination of $\Psi_0^*$ will improve the accuracy of $\tau$ obtained from fitting experimental data, using the results of the mathematical description described by (9). A possible method to achieve this is by measuring the diffuse reflection coefficient of the turbid medium and then use the expressions for fluence rates and escape functions presented by Gardner *et al* (1996). These expressions are only a function of the diffuse reflection coefficient and thus $\Psi_0^*$ can be calculated rapidly.

The estimation of the actual fluence rate profile and escape function by exponentially decaying functions are coarse simplifications. Especially the fluence rate profile may differ a great deal from this exponent when the curvature of $\Psi^*(z)$ is small and the maximum lies deeper in the medium. This is the case when longer wavelengths are used for excitation.

The solutions of (6) lie in a defined region of the $\mathcal{F}_n(t)$, $t$-plane as can be seen from figure 6 where $\mathcal{F}_n(t)$ is plotted as a function of a dimensionless time $\theta = \Psi_0^*(t/\tau)$. The region is enclosed by the functions $\mathcal{F}_0(t)$ and $\mathcal{F}_\infty(t)$. A few analytical solutions from (9) are drawn. It can be shown from numerical calculations that all $\mathcal{F}_n(t)$ with $n \geqslant 0$ lie in this region. Furthermore with increasing $n$, $\mathcal{F}_n(t)$ gradually approaches $\mathcal{F}_\infty(t)$.

Since the effective attenuation coefficient for light in tissue normally decreases with

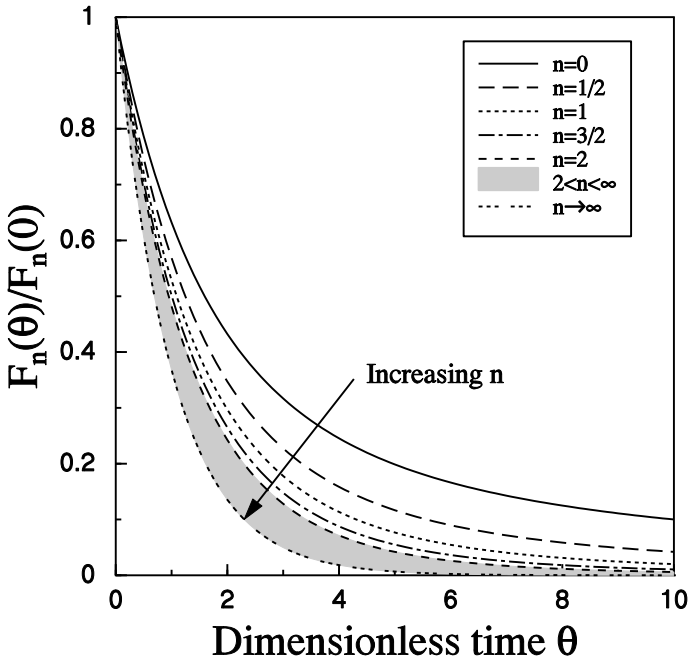


**Figure 6.** Graphical representation of all analytic solutions given by (9). The relative fluorescence signal is plotted as a function of the dimensionless time $\theta = \Psi_0^*(t/\tau)$. As $n$ increases the functions begin to resemble each other as indicated by the shaded area within which all solutions for $2 < n < \infty$ lie.

increasing wavelength, the ratio of the effective attenuation coefficients for the detection and excitation light $n$ will lie between 0 and 1 in most practical cases. We see from figure 6 that in this region there are only few analytical solutions. This implies that if we try to fit measured data where the actual ratio $n$ equals, e.g., 0.3 with the analytical solution for $n = \frac{1}{2}$, the resulting value for $\Psi_0^*/\tau$ is not a good indication of the actual value. In such a case it is better to use the results of (13).

No assumptions were made about $n$ to derive (13), thus it holds for all $n \in \mathbb{R}$. If $\mathcal{A}$ and $n$ are known definitely, we only need to look at the initial decrease of the fluorescence signal to determine a more reliable value for $\Psi_0^*/\tau$. Complete fitting of the curve using one of the solutions in (9) is, however, no longer possible if $n$ or $(n + \frac{1}{2}) \notin \mathbb{N}$.

Obviously, it is also possible to fit the initial decrease of a measured fluorescence signal with a single-exponential function. This will result in a value for $\Psi_0^*/\tau$ that equals $-\partial(F(t)/F(0))/\partial t$, assuming correction of the measured data for the autofluorescence component $\mathcal{A}$. Comparing this with the value for $\Psi_0^*/\tau$ that will be obtained when fitting the initial decrease with (13) we see that there is a factor $(n+1)/(n+2)$ difference between these two calculated values. Hence fitting with a single-exponential function implies that the estimation for the bleaching time $\tau$ is a factor $(n+2)/(n+1)$ too high.

The assumption of an initial homogeneous photosensitizer distribution $C_0$ made in section 2 is not sure to be met in all practical cases. Unfortunately it is a necessary assumption to make (6) analytically solvable. But it is obvious that if the initial photosensitizer distribution is not homogeneous the $\mathcal{F}(t)$ can still not be described by a single-exponential function.

In section 3 the term autofluorescence is introduced as being the non-bleachable

part of the fluorescence signal related to the intrinsic tissue fluorescence. Bleaching of the autofluorescence has also been reported (Zeng *et al* 1993) but in these studies the used excitation wavelength is normally shorter than 630 nm. If we want to incorporate the possibility of autofluorescence bleaching in the presented model, we have to use a composition of (9) with different bleaching times $\tau$. Since the used mathematical description describes the measured data well, the presence of an additional bleachable fluorescent component is unlikely. Should there be one, then the bleaching time of this component will be large compared to the $\tau$ of the photosensitizer and hence have little effect on the calculated bleaching dose constant $\beta$.

## 6. Conclusions

The main purpose of the work discussed in this paper was to investigate how the photobleaching signal is influenced by tissue properties. Comparison of numerical calculations using results from MC simulations and the expression for the relative fluorescence signal given in (9) showed that the mathematical description presented describes the time dependence of the fluorescence signal as observed during fluorescence measurements *in vivo* accurately. It uses only one bleaching time constant corresponding to one bleachable component.

Fluorescence measurements performed on patients and rats were evaluated with the results of the mathematical description, indicating the bleaching dose constant $\beta$ for PpIX to be $33 \pm 3$ J cm$^{-2}$.

## Acknowledgment

This work was supported by the Dutch Technology Foundation (STW, project number AGN 44.3413).

## Appendix. Analytic solutions for equation (8)

Recall the integral equation for the resulting fluorescence light given by (8)

$$\mathcal{F}(t) = \int_0^\infty \exp\left[-(\mu_e + \mu_d)\, z\right] \exp\left[-\Psi_0^*(t/\tau)\, e^{-\mu_e z}\right] dz \left\{ \int_0^\infty \exp\left[-(\mu_e + \mu_d)\, z\right] dz \right\}^{-1}. \quad \text{(A1)}$$

There is no general closed form solution for this equation. However, it will be shown that if we substitute $\mu_e = \mu$ and $\mu_d = n\mu_e = n\mu$, where $n$ is positive, analytic solutions are possible for some discrete cases.

Performing this substitution (A1) yields

$$\mathcal{F}_n(t) = \int_0^\infty \exp(-\mu z) \exp\left(-\theta\, e^{-\mu z}\right) \exp(-n\mu z)\, dz \left\{ \int_0^\infty \exp\left[-(n+1)\, \mu z\right] dz \right\}^{-1} \quad \text{(A2)}$$

where we also substituted $\Psi_0^*(t/\tau)$ by $\theta$ for clarity reasons.

The denominator of this fraction representing $F_n(0)$ is easily seen to result in

$$F_n(0) = \int_0^\infty \exp\left[-(n+1)\, \mu z\right] dz = \left[(n+1)\, \mu\right]^{-1}. \quad \text{(A3)}$$

This leaves us with solving the numerator of the fraction in (A2) which represents $F_n(t)$.

*Recursive equation*

Using

$$\int \exp(-\mu z)\exp\left(-\theta\,\mathrm{e}^{-\mu z}\right)\mathrm{d}z = (\mu\theta)^{-1}\exp\left(-\theta\,\mathrm{e}^{-\mu z}\right), \tag{A4}$$

partial integration of $F_n(t)$ yields

$$F_n(t) = (\mu\theta)^{-1}\exp\left(-\theta\,\mathrm{e}^{-\mu z}\right)\exp(-n\mu z)\Big|_0^\infty + n\,(\theta)^{-1}\int_0^\infty \exp\left(-\theta\,\mathrm{e}^{-\mu z}\right)\exp(-n\mu z)\,\mathrm{d}z. \tag{A5}$$

The integral in (A5) can be identified as $F_{n-1}(t)$. Using this and inserting the limits in (A5) yields

$$F_n(t) = n\,(\theta)^{-1}\,F_{n-1}(t) - (\mu\theta)^{-1}\exp(-\theta). \tag{A6}$$

No assumptions, other than that $n$ is positive are made to derive this recursive equation. Therefore closed form solutions of (A1) can be obtained if $F_m(t)$ is known for $0 \leqslant m < 1$. There are only two cases found for which there is an analytic solution for $F_m(t)$, i.e. $m = 0$ and $m = \frac{1}{2}$. Although not mathematically proven we are confident that these two are the only analytic solutions.

*Closed form solution of (A6) for n an integer*

Considering $n$ in (A6) to be an integer means that we have to determine $F_0(t)$ in order to obtain a general closed form solution for all $n \in \mathbb{N}$. Setting $n$ in the numerator of (A2) to zero gives

$$F_0(t) = \int_0^\infty \exp(-\mu z)\exp\left(-\theta\mathrm{e}^{-\mu z}\right)\mathrm{d}z = (\mu\theta)^{-1}\left[1-\exp(-\theta)\right]. \tag{A7}$$

We can now expand (A6) until $F_n(t)$ is only a function of $F_0(t)$ and insert the result of (A7). When organizing terms this yields

$$F_n(t) = (\mu)^{-1}\,\frac{n!}{\theta^{n+1}}\left[1-\exp(-\theta)\right] - \frac{\exp(-\theta)}{\mu\theta}\sum_{k=0}^{n-1}\frac{n!}{(n-k)!}\left(\frac{1}{\theta}\right)^k. \tag{A8}$$

Finally we divide this expression with the result of (A3) to obtain the closed form solution of (A2) for $n \in \mathbb{N}$ as presented (9).

*Closed form solution of (A6) for $(n + \frac{1}{2})$ an integer*

Another analytic solution of $F_m(t)$ for $0 \leqslant m < 1$ is found for $m = \frac{1}{2}$. Substituting $n = \frac{1}{2}$ in the numerator of (A2) and performing a partial integration gives

$$F_{\frac{1}{2}}(t) = (\mu\theta)^{-1}\exp\left(-\theta\,\mathrm{e}^{-\mu z}\right)\exp\left(-\tfrac{1}{2}\mu z\right)\Big|_0^\infty + (2\theta)^{-1}\int_0^\infty \exp\left(-\tfrac{1}{2}\mu z\right)\exp\left(-\theta\,\mathrm{e}^{-\mu z}\right)\mathrm{d}z. \tag{A9}$$

Because

$$\int_0^\infty \exp\left(-\tfrac{1}{2}\mu z\right)\exp\left(-\theta\,\mathrm{e}^{-\mu z}\right)\mathrm{d}z = \sqrt{\pi/\theta}\,(\mu)^{-1}\ \mathrm{erf}\left(\sqrt{\theta}\right) \tag{A10}$$

where erf() denotes the tabulated error function, this results in

$$F_{\frac{1}{2}}(t) = \tfrac{1}{2}\sqrt{\pi/\theta}\,(\mu\theta)^{-1}\ \mathrm{erf}\left(\sqrt{\theta}\right) - (\mu\theta)^{-1}\exp(-\theta)\,. \tag{A11}$$

Again expanding (A6) but now until $F_n(t)$ is only a function of $F_{\frac{1}{2}}(t)$ yields

$$F_n(t) = (\mu)^{-1}\,\frac{(2n)!!}{2^{n-\frac{1}{2}}\theta^{n+1}}\sqrt{\pi}\ \mathrm{erf}\left(\sqrt{\theta}\right) - \frac{\exp(-\theta)}{\mu\theta}\sum_{k=0}^{n-\frac{1}{2}}\frac{(2n)!!}{(2n-2k)!!}\frac{1}{2^k}\left(\frac{1}{\theta}\right)^k. \tag{A12}$$

Dividing this equation by (A3) results in the general closed form solution of $F_n(t)$ for $(n+\frac{1}{2}) \in \mathbb{N}$ given in (9).

## References


Boyle D G and Potter W R 1987 Photobleaching of photofrin II as means of eliminating skin photosensitivity *Photochem. Photobiol.* **46** 997–1001

Cheong W F, Prahl S A and Welch A J 1990 A review of the optical properties of biological tissues *IEEE J. Quantum Electron.* **26** 2166–85

Dietel W, König K and Zenkevich E 1990 Photobleaching of HpD fluorescence and formation of photoproduct *in vivo* and in solution *Lasers Life Sci.* **3** 197–203

Gardner C M, Jacques S L and Welsch A J 1996 Light transport in tissue: accurate expressions for one-dimensional fluence rate and escape function based upon Monte Carlo simulation *Lasers Surg. Med.* **18** 129–38

Grossweiner L I 1991 Light dosimetry model for photodynamic therapy treatment planning *Lasers Surg. Med.* **11** 165–73

Jacques S L, Joseph R and Gofstein G 1993 How photobleaching affects dosimetry and fluorescence monitoring of PDT in turbid media *Optical Methods for Tumor Treatment and Detection, SPIE* vol 1881 (Bellingham, WA: SPIE) pp 168–79

Kennedy J C and Pottier R H 1992 Endogeneous protoporphyrin IX, a clinically useful photosensitizer for photodynamic therapy *J. Photochem. Photobiol.* B **14** 275–92

König K, Wabnitz H and Dietel W 1990 Variation in the fluoresence decay properties of haematoporphyrin derivative during its conversion to photoproducts *J. Photochem. Photobiol.* B **8** 103–11

Mang T S, Dougherty T J, Potter W, Boyle D G, Somer S and Moan J 1987 Photobleaching of porphyrins used in photodynamic therapy and implications for therapy *Photochem. Photobiol.* **45** 501–6

Moan J 1986 Effect on bleaching of porphyrin sensitizers during photodynamic therapy *Cancer Let.* **33** 45–53

——1988 A change in the quantum yield of photoinactivation of cells observed during photodynamic treatment *Lasers Med Sci* **3** 93–7

Potter W R and Mang T S 1984 Photofrin II levels by *in vivo* fluorescence photometry *Porphyrin Localization and Treatment of Tumors* ed D R Doiron and C J Gomer (New York: Liss) pp 91–114

Potter W R, Mang T S and Dougherty T J 1987 The theory of photodynamic therapy dosimetry: consequences of photodestruction of sensitizer *Photochem. Photobiol.* **46** 97–101

Roberts W G, Smith K M, McCulloug J L and Berns M W 1989 Skin photosensitivity and photodestruction of several potential photodynamic sensitizers *Photochem. Photobiol.* **49** 431–8

Star W M 1997 Light dosimetry *in vivo Phys. Med. Biol.* **42** 763–87

Svaasand L O and Potter W R 1992 The implications of photobleaching for photodynamic therapy *Photodynamic Therapy: Basic Principles and Clinical Aspects* ed B Henderson and T J Dougherty (New York: Dekker) pp 369–84

Zeng H, MacAulay C, Palcic B and McLean D I 1993 Laser-induced changes in autofluorescence of *in vivo* skin *Laser–tissue Interaction IV, SPIE* vol 1882 (Bellingham, WA: SPIE) pp 278–90